Charging Electric Vehicle Batteries: Wired and Wireless Power Transfer

Exploring EV charging technologies

by Hua (Kevin) Bai, Daniel Costinett, Leon M. Tolbert, Ruiyang Qin, Liyan Zhu, Ziwei Liang, and Yang Huang

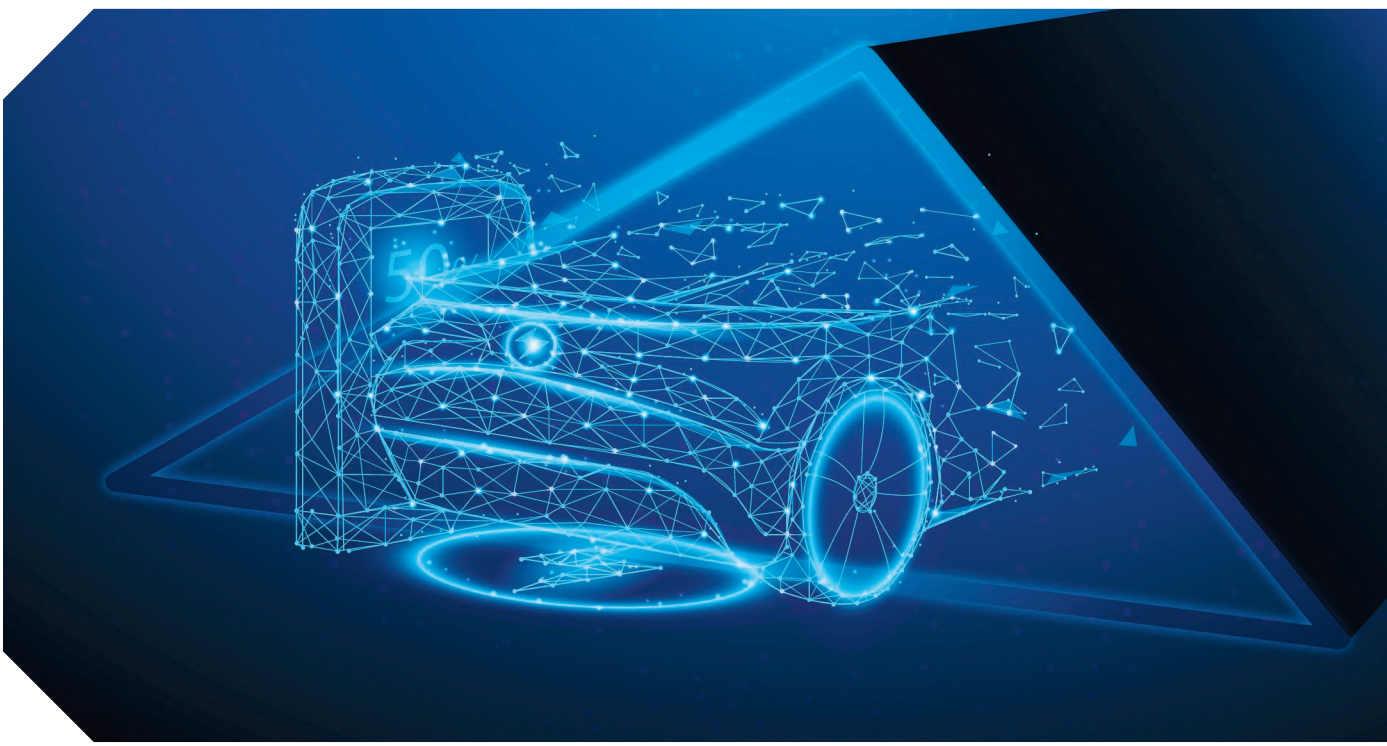

Due to the environmental concerns about CO_2-caused global warming, policymakers are pushing electrified vehicles (EVs) to reduce these emissions. For passenger vehicles only, the electrified fleet is forecasted to reach 80 million in the U.S. and 500 million globally by 2040. Key enablers for such rapid EV adoption include the improvement of battery energy density, lifespan and safety, and drastic cost reduction of batteries and power electronics. The technology of power electronics nowadays can be found in many aspects of EVs. It alters and transforms the energy from the power source to different forms to feed the loads. For example, the on-board charger (OBC) accepts ac input and converts it to high voltage (HV) dc to charge the propulsion battery. An auxiliary power module (APM) steps down the HV battery voltage to low voltage (LV) to charge the LV battery [1].

Digital Object Identifier 10.1109/MPEL.2022.3173543
Date of current version: 16 June 2022

2329-9207/22©2022IEEE

The HV dc bus voltage is converted to an ac form to drive the propulsion motor, forming the motor drive inverter. Putting the power electronics system and the batteries together, the typical structure of an EV is shown in Figure 1. In addition, power electronics can be found in other onboard auxiliary circuits, such as LED lighting and battery management system (BMS).

As shown in Figure 2, a typical OBC includes a power factor correction (PFC) stage and an isolated dc/dc stage. Such a two-stage design can effectively decouple the grid from the vehicle. Certainly the efficiency, weight and size will all receive the penalty of this two-stage design, particularly given the existence of the dc-link capacitors and galvanic transformer. Therefore it is not hard to understand why in recent years both academia and EV industries put vast efforts into its potential improvement.

The PFC stage maintains unity power factor at the ac input port and reduces the injection of harmonics and reactive power to the grid. Otherwise, the utility company will tax this "dirty power" drawn from the grid. While specifications might vary due to different companies' requirement, usually it is demanded that at full power the grid power factor is >0.99 while the grid current total harmonic distortion (THD) is <5% or even lower. A dc/dc stage is then inserted between the PFC stage and batteries, to provide isolation and accommodate the wide output voltage range. Depending on the state of charge (SOC), the terminal voltage of a 400 V-rated battery can vary from 250 V to 450 V [2], or 550 V to 850 V for an 800 V-rated battery [3]. The isolation is necessary by the regulation of standard IEC 61851-1 for safety concerns [4]. Different from the data-center ac/dc power supply which also has a similar topology, EV battery chargers usually face wider output voltage, and sometimes wider ac input voltage range. A recent trend is the emergence of universal OBCs, which accommodates both single-phase (100~260 Vac) and three-phase (208~500 Vac) input. Such requirements usually yield redundancy of the design. Given that the automotive industry is very cost sensitive, engineers must find a balance between performance and cost, particularly when designing such universal chargers.

The charging technology, in the long term, needs to expedite the charging speed of the battery in order to compete with the short time it takes for fuel pumping to fill the tank in conventional vehicles. The OBCs can then be classified into several levels in terms of their power ratings. Essentially, it is based on the grid voltage and current rating of the circuit breaker. In the U.S., the charging power from the residential power outlet can be classified into three levels according to SAE J1772 [5]. The commonly used rating series are 3.3 kW, 6.6 kW, 11 kW, 19.2 kW and 22 kW for OBCs only. When going to higher power, the large size and cost will become an obstacle to place the OBC inside the vehicles. Therefore chargers with much higher power rating, say >22 kW, are placed outside the vehicle and categorized as off-board chargers, e.g., dc fast charging, where a dc instead of ac input is provided. Fast chargers and extreme fast chargers (XFC >150 kW) are usually off-board chargers. Lead by Chinese and Japanese companies, a super charging technology to provide 900 kW charging power (Chaoji) can be expected in the near future, which allows customers to complete charging in a few minutes instead of hours. Due to its high power, such charging infrastructure is serving for public purpose.

As a global EVSE supplier, Brusa has been developing a series of EV chargers, from 3.3 kW to 22 kW. Their 22 kW OBC (NLG664) exhibits 94% efficiency and 2 kW/L power density. Academic effort in recent years is trying to improve both efficiency and power density. Shown in Figure 3(a) below is a 22 kW EV offboard charger prototype, developed by the University of Tennessee, Knoxville (UTK) power electronics group. Its charging I-V curve is shown in Figure 3(b).

The internal view of the charger reveals that a significant volume of EV charger is occupied by passive components (capacitors, inductors, electromagnetic interference (EMI) filters, heatsink, etc). One solution lies in the recent rapid adoption of wide-bandgap (WBG) devices, such as silicon carbide (SiC) and gallium nitride (GaN). Such semiconductor switches compared to the traditional silicon (Si) devices have faster switching transitions and less switching loss, which cuts the loss and thereby reducing the heatsink size and can be operated at higher switching frequency resulting in less inductor and capacitor usage. This directly benefits the power density. On the other hand, we also need to understand WBG devices are not the solution to all challenges. For instance:

1) *Universal AC input.* When the grid side is single-phase ac input, we can assume the grid voltage is

$$v_g(\mathrm{t}) = V\cos(\omega t) \tag{1}$$

With unity power factor, the ac current is

$$i_g(\mathrm{t}) = I\cos(\omega t) \tag{2}$$

Therefore the input power is

$$p_g(\mathrm{t}) = VI\cos^2(\omega t) \tag{3}$$

which can be translated into

$$P_g(t) = \frac{VI}{2}\{1+\cos(2\omega t)\} \tag{4}$$

Therefore the grid power exhibits a double-line frequency component, e.g., 120 Hz when operated with 60 Hz grid. Filtering out such low-frequency component cannot be answered by WBG devices, but instead a large dc-link capacitor. Some attempts have been made to minimize the dc-link capacitance and let such double-line-frequency power flow toward the battery, which usually is not welcome by EV original equipment manufacturers (OEMs). Therefore the single-phase and universal chargers yield much lower power density than a three-phase charger, even with WBG devices.

2) *Magnetics design.* EV chargers provide opportunities to magnetics (inductor and transformer) companies. The desire of having compact, light, and efficient magnetics is increasing, which imposes new challenges. Theoretically, the higher the switching frequency, the smaller the inductance. When inductance is small enough, we can then lay out the inductor/transformer windings on printed circuit boards (PCB), wrapping a small core, forming a so-called planar transformer. Such technology greatly flattens the transformer footprint thereby saving overall volume. The challenge, however, is once the windings are stacked closely, the turn-to-turn capacitance, and the capacitance between primary and secondary windings will be increased significantly. Shown in Figure 4(a) is an equivalent circuit of a transformer when considering all such parasitic capacitance. Coupled with fast switching transitions of WBG devices, such capacitance can generate some unexpected electrical waveforms; also, a large capacitance between primary and secondary windings (C_{ps}) forms a path of EMI noise to flow between the grid side and the battery side.

Authors have integrated a planar transformer into a nonresonant circuit, dual active bridge (DAB) converter when the switching leg output is directly tied to the transformer. When the dc/dc stage input voltage is 400 V, Figure 4(b) shows the experimental waveform. Here, the brown curve is the primary voltage, the blue one is the secondary voltage, green is the primary current and the purple is the secondary current. A significant current oscillation is observed at the transformer secondary-side current. It turned out that the winding capacitance is the reason. A 3 nF capacitance is measured across the secondary-side winding of the physical transformer. Such high-frequency oscillation creates concerning EMI and additional loss to both switches and the transformer.

Therefore, WBG devices are not the only answer to EV charger improvement. In some cases, a mismatch between WBG and other peripheral components can yield even worse performance. Particularly in recent years, low power OBC development has matured significantly. Convincing OEMs to use different switches with a new design can face obstacles.

On the other hand, when we step back and consider the whole EV system, another approach to save cost and size can be traced back to better system-level integration and optimization. One typical example is integrating the OBC

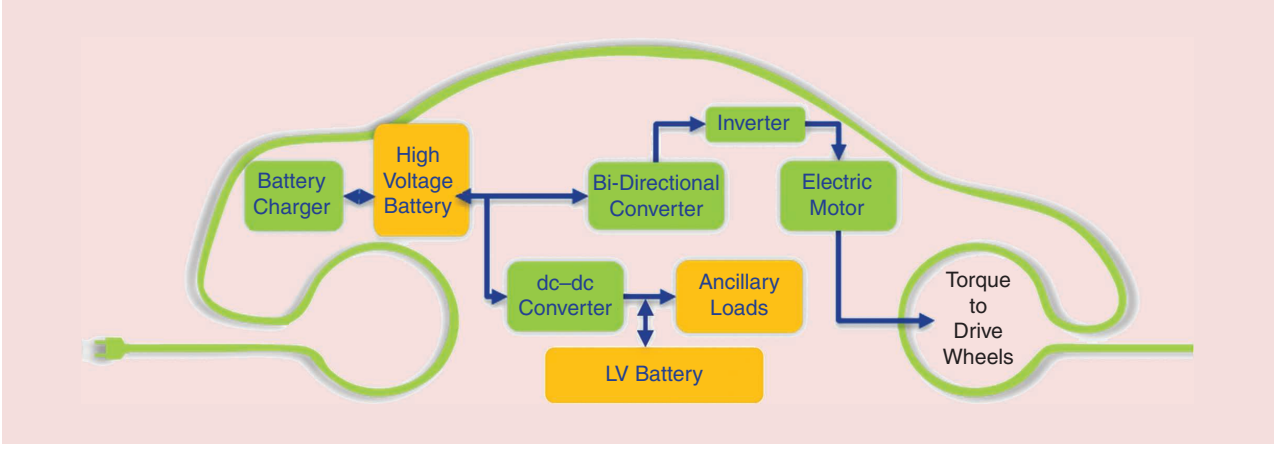

FIG 1 Typical structure of an EV.

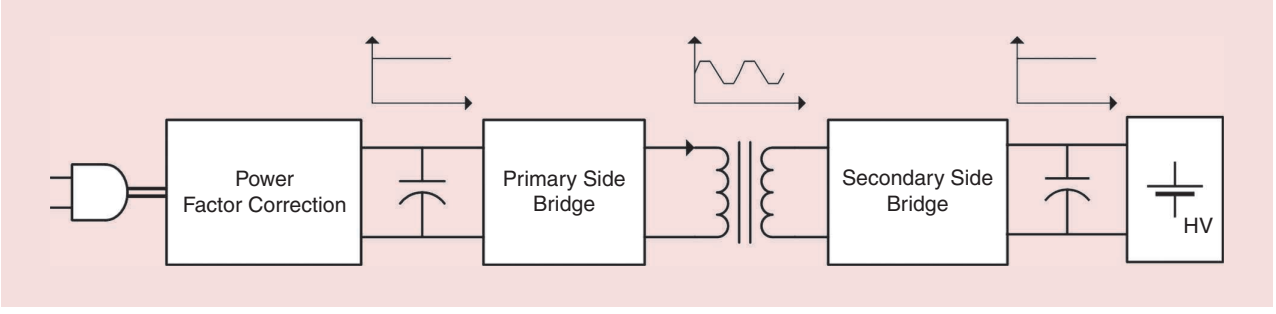

FIG 2 Typical structure of the OBC.

with the APM. The APM in an EV is mainly used to replace the alternator in a conventional internal combustion engine (ICE) vehicle. It bridges the HV system with the LV system, say 12 V. Essentially, it is another isolated dc/dc converter, with the typical structure very similar to the isolated dc/dc stage of the OBC[6], except that the terminal voltage varies from 10 V to 14 V [7], [8]. This provides opportunities for two units to share the same components aiming at cost saving and size reduction.

In addition to the system integration, recent EV users tend to treat the battery not only as the load, but also as a generation source. While vehicle-to-grid (V2G) has concerns for EV OEMs in regards to battery degradation due to overuse, vehicle-to-load (V2L) feature is useful during grid blackout particularly when in recent years natural disasters have happened more frequently. This, however, requires the battery charger to be bidirectional and have the ability for grid forming control, which will add cost to the charger design. Such a feature allows the battery together with the OBC to form a local microgrid.

The third element is the transformer-less design for XFCs. Such high charging power, e.g., >150 kW, imposes high current stress on the distribution-level power grid, particularly when considering several EVs are being charged at the same time. Therefore the latest research attempt is to draw power directly from medium voltage transmission lines, say 13.4 kVac. Instead of stepping down such voltage to three-phase 480 Vac using bulky and heavy 50/60 Hz transformer, high-voltage semiconductor devices with multilevel topologies offer the chances to eliminate the grid-side transformer thereby saving size and weight.

Last but not the least, wireless power transfer (WPT) is another hotspot emerging in recent years. The wireless charging coils can be buried underground, allowing the charging station footprint to be reduced. Charging plugs, which cause safety concerns without supervision and can be easily damaged, are no longer required. In October 2020, SAE International published its first standard J2954 on WPT for EVs, allowing charging power up to 11 kW over a

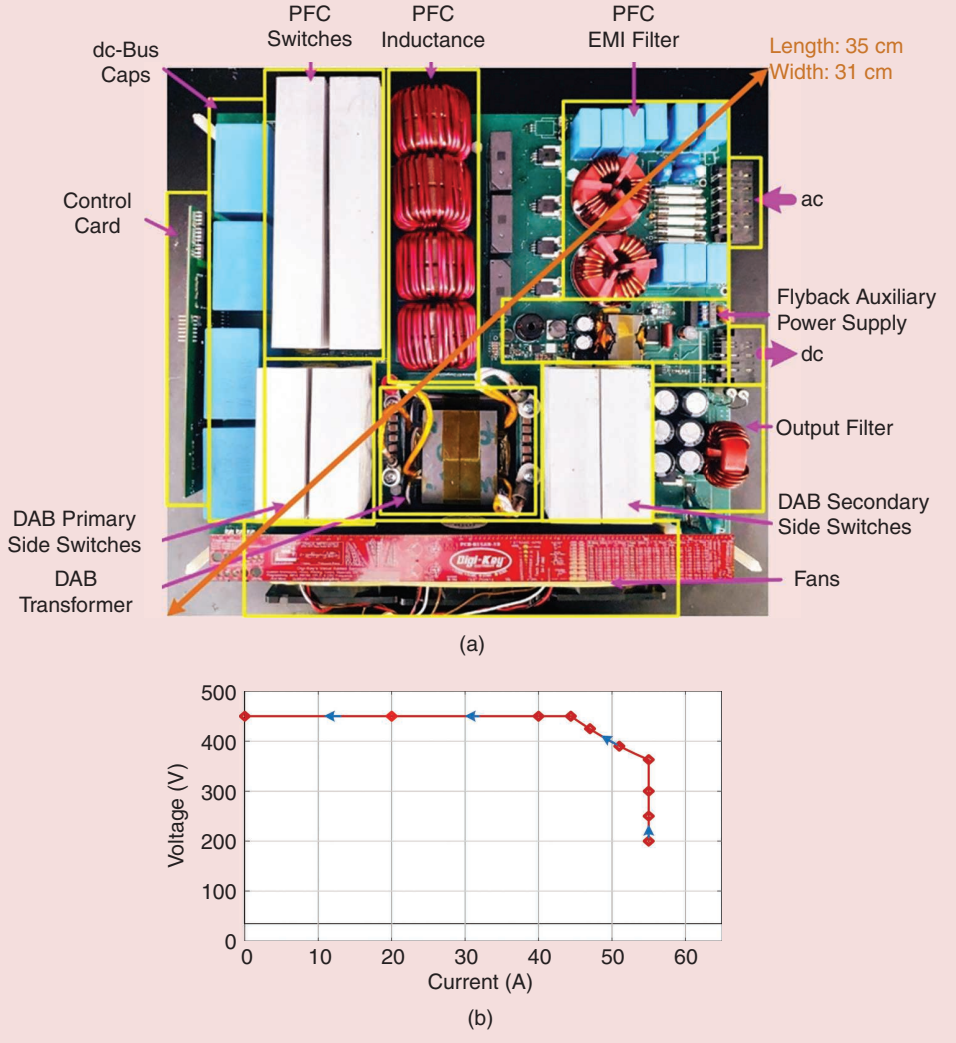

FIG 3 (a) UTK designed 22 kW EV battery charger. (b) Charging I-V curve specifications for 22 kW EV battery charger.

250 mm air gap with up to 94% system efficiency. The standard also outlines the parking assistance for EV that makes autonomous parking and charging available. Together with J2954, J2847/6 is also published recommending the communication protocols between EVs and charging stations. Based on the different coupling mechanisms between transmitter side and receiver side of the WPT system, there are two types of candidate WPT techniques for high-power, near-field wireless EV applications: Inductive Power Transfer (IPT) and Capacitive Power Transfer (CPT), which will be compared in this paper in a later section.

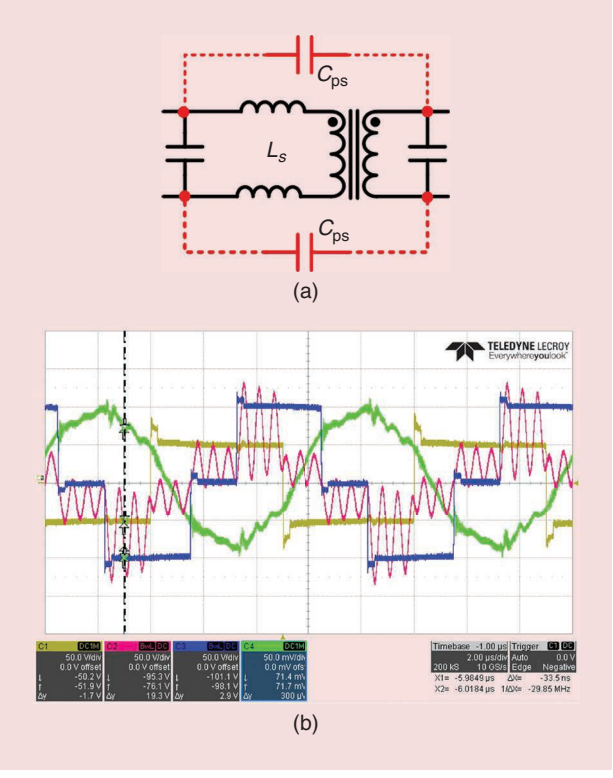

FIG 4 (a) Equivalent circuit of the transformer. (b) Transformer oscillation (experiments).

High-level System Integration

Take the integration of OBC+APM as an example. Different from OBC only working at the charging mode, the APM usually works continuously. Even when the vehicle is fully stopped, the APM still needs to power the LV system for the nonpropulsion loads, such as control units and cooling system[9]. One typical structure of the integrated charger is shown in Figure 5, using a three-winding transformer. In this way, grid, HV and LV batteries are all isolated from each other. Active bridges then allow the power to flow through three ports freely.

An exemplary design is shown in Figure 6(FIG 6a), forming a phase-shift (PS)-triple port converter (TPC). Three active bridges are connected to three isolated power sources through a three-winding high-frequency transformer, respectively. The power flow of each port is then controlled by the phase difference among all ports. The two-level voltage generated from the bridges together with the leakage inductance network forms an equivalent circuit shown in Figure 6(b). Phase shifts and impedance among sources are the two key factors to determine the power flow.

One key challenge for such an integration approach is that the power of one port is coupled with the other two. The second challenge lies in the LV side. Assuming 2.5 kW is needed for the 12 V battery, the LV bridge will conduct >200 A average current, with the peak current of the related winding being >400 A. While more semiconductor switches can be paralleled to offset the conduction loss, switching off such large current can be the challenge, particularly considering the switching loss and the accompanying EMI. Last but not least, the turns ratio of the transformer can be high, say 400 V:400 V:12 V.

To overcome all the shortcomings mentioned above, UTK power electronics team worked with Hella and proposed a novel current-fed three-port converter, as shown in Figure 7(a) [12]. Without considering the ac/dc stage, the converter has three ports: the primary side, HV side, and LV side, being connected to the PFC output, HV battery, and LV

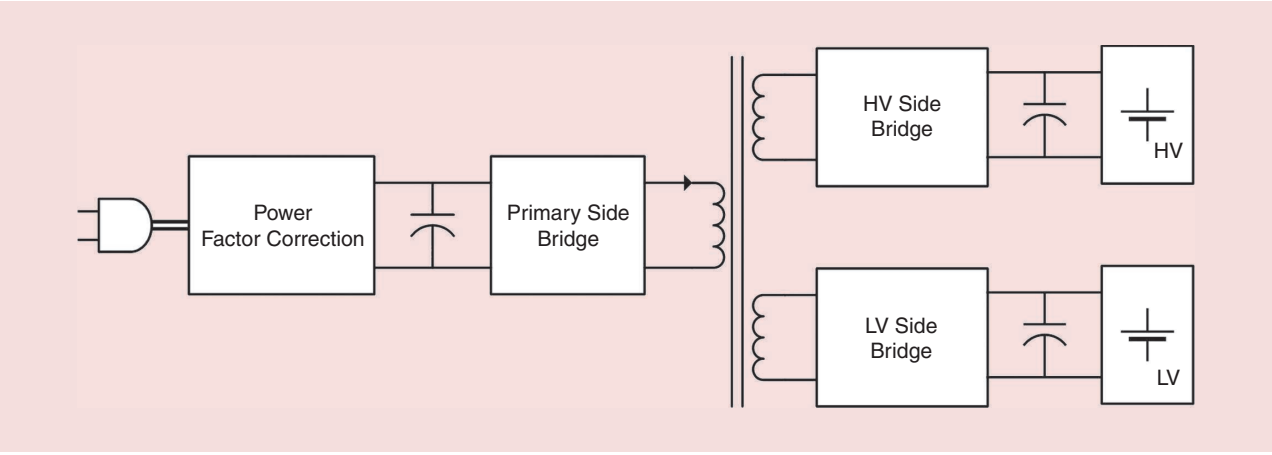

FIG 5 Integration of OBC and APM.

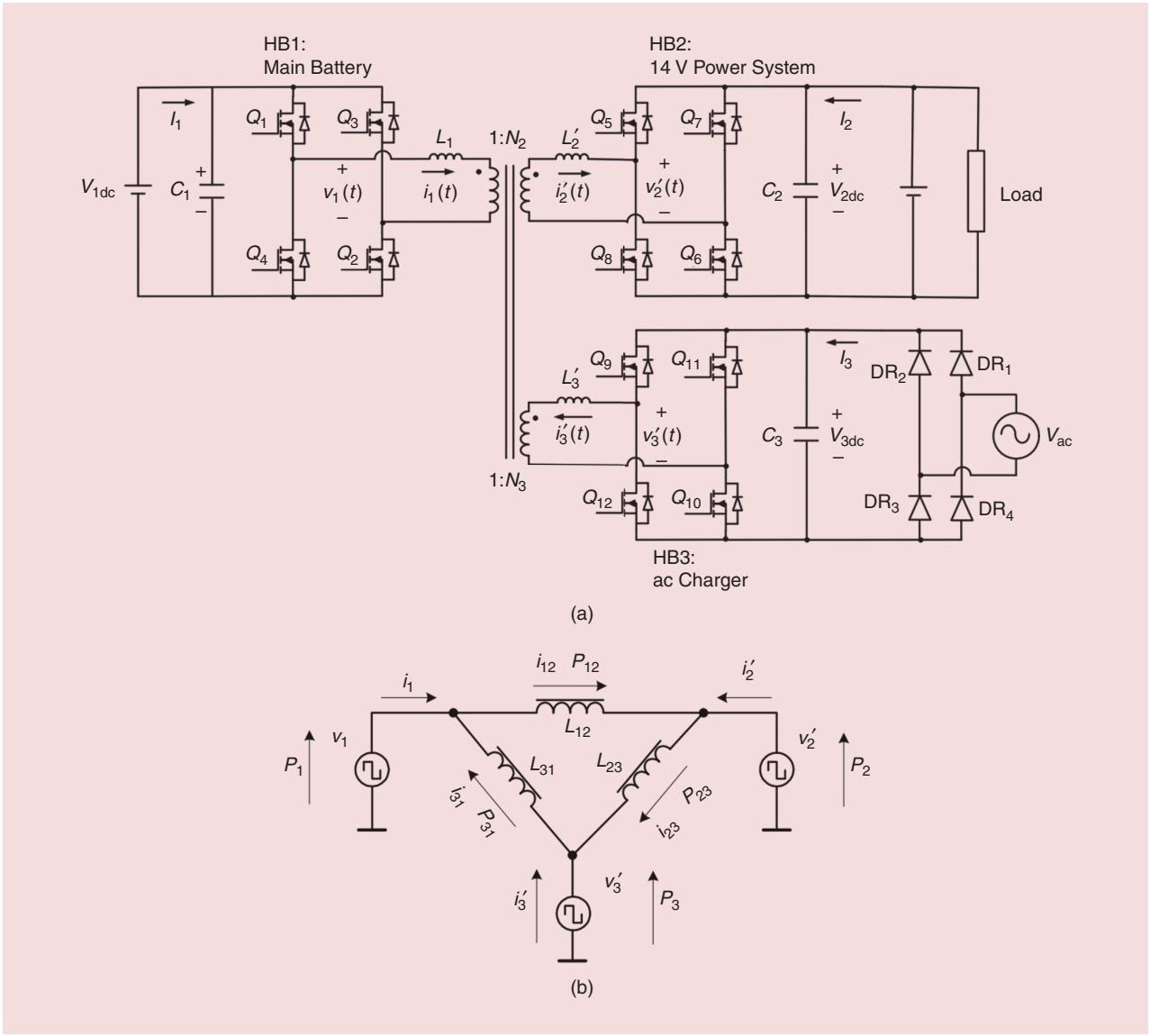

FIG 6 (a) Basic structure of the PS-TPC [11]. (b) The equivalent circuit model for PS-TPC [11].

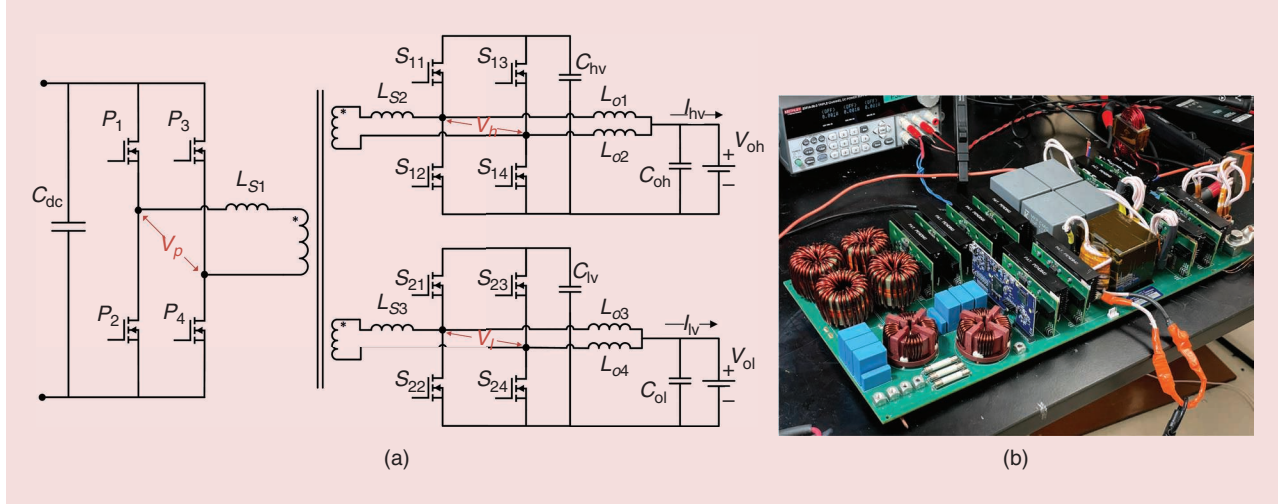

FIG 7 (a) Topology of the UTK/Hella converter for the integrated charger. (b) Prototype of the integrated OBC+DCDC.

battery, respectively. L_{s1}~L_{s3} are the leakage inductances of the three windings of the transformer, respectively. L_{01} and L_{02} are negatively coupled inductors for HV output filter. The same design applies for L_{03} and L_{04} at the LV output. C_{hv} and C_{lv} are clamping capacitors and used to maintain a high dc voltage to reduce current stress on both transformer secondary sides. An exemplary prototype is also shown in Figure 7(b). The rationale behind this design is that the current-fed port boosts the LV side voltage to a much higher value, which significantly reduces the turns ratio thereby facilitating the transformer design. In addition, duty cycles are introduced as additional control freedoms, enabling the possibility of further optimization, e.g., realizing zero-voltage-switching (ZVS) in most of the power range. Even though the debate of pros and cons of voltage source and current source converter continues, and the current-fed topology is nothing new, such integration attempt actually brings two types of converter technologies together by maximizing their potential at the same time.

Using Battery and OBC for V2L

When the grid loses power during a blackout, one mission of the EV battery and OBC is to form the local grid and provide minimum energy usage. It then requires the energy to flow from vehicle to the grid created by the vehicle power supply; this operation can be called vehicle to load (V2L). A typical topology is shown in Figure 8(a). At the ac side, a conventional three-phase four-wire inverter is a promising candidate. At the dc-bus side, there are split dc-link capacitors C_{N1} and C_{N2}, where the midpoint of the split dc-link capacitors serves as the neutral point. The fourth leg is formed by S_{n1} and S_{n2}, should a two-level topology be preferred. L_N aids in the regulation of the neutral-point voltage caused by the load imbalance. L_f and C_f are the grid-side filter inductor and capacitor, respectively. Note the fourth leg might not be necessary such as in the case where the dc-link capacitor tank is large enough to cope with a large neutral current. With the fourth leg stabilizing the neutral point, each phase can be essentially equivalent to a buck converter and controlled independently with conventional SPWM, with the equivalent circuit of each phase shown in Figure 8(b). In this way three independent phases, A, B and C are formed. Each phase can then undertake balanced or unbalanced load, should the neutral point be controlled well.

Potentially, when $R_L \to \infty$, i.e., no-load, the overall grid inverter part of the OBC is supplying just the LC circuit, which has a natural resonant frequency. If the OBC output at the ac side happens to have a voltage component around such resonant frequency, large voltage and current harmonics are expected on the phase output, deteriorating the grid power quality. Note such operational mode is not V2G, which has the normal utility power grid connected. V2L function requires the battery and charger to form its own microgrid, therefore from the control point of view it can be more challenging than V2G. One approach is controlling the effective output impedance of the converter, which

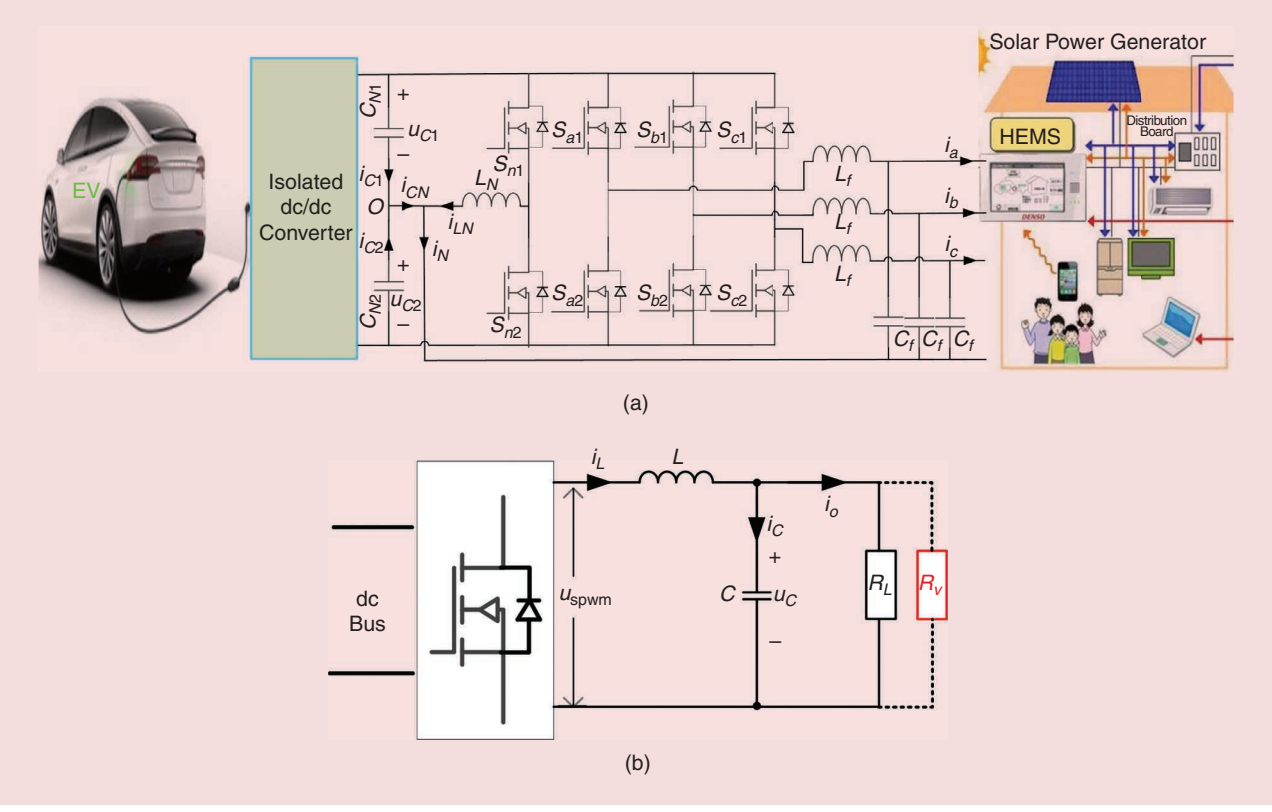

FIG 8 (a) A three-phase four-wire inverter used in a V2L EV charger. (b) Equivalent circuit of each phase with virtual resistor.

assumes a virtual resistor R_v is in parallel to the load resistor R_L, as highlighted in Figure 8(b). The essence of employing such an imaginary resistor is optimization of the system transfer function by adding a notch filter to suppress the harmonics. Simulation results are shown in Figure 9. With the virtual resistance, the quality of both grid voltage and current is improved.

Transformerless XFC Design

To complete battery charging in a short time period, power levels of at least 350 kW and up to 1 MW are needed for conventional passenger vehicles. In North America, Electrify America, a subsidiary of Volkswagen Group of America, was established in late 2016. It opened California's first 350 kW charger location in December 2018. 350 kW chargers are now available in front of more than 120 Walmart stores. Electrify America now offers stations widely available so that 96% of Americans live within 120 miles of a charger.

Take Tesla Model 3 as an example. The vehicle is equipped with a 75 kWh battery, which requires >12 hr to charge if only a 6.6 kW OBC is utilized. However, with a 500 kW XFC, the charging time can be shortened to ~10 mins, which certainly helps to expedite EV adoption and use of these vehicles for longer trips. These high-power levels, however, are comparable to small electric utility substations, especially for a location that has multiple XFCs to charge multiple vehicles simultaneously. Therefore, most proposed designs involve the primary of the charger system connected to an electric utility's distribution system at a medium voltage (MV) (e.g., 12.4, 13.2, 13.8 kV). The XFC then must step down the MV to a voltage level compatible with the battery pack (200 to 400 V) and regulate the voltage and current in the charging process. At the present time, >500 kW XFC is still uncommon. EVs capable of accepting 350 kW charging power typically use an 800 V battery, for instance, Porsche Taycan and Audi e-tron GT started

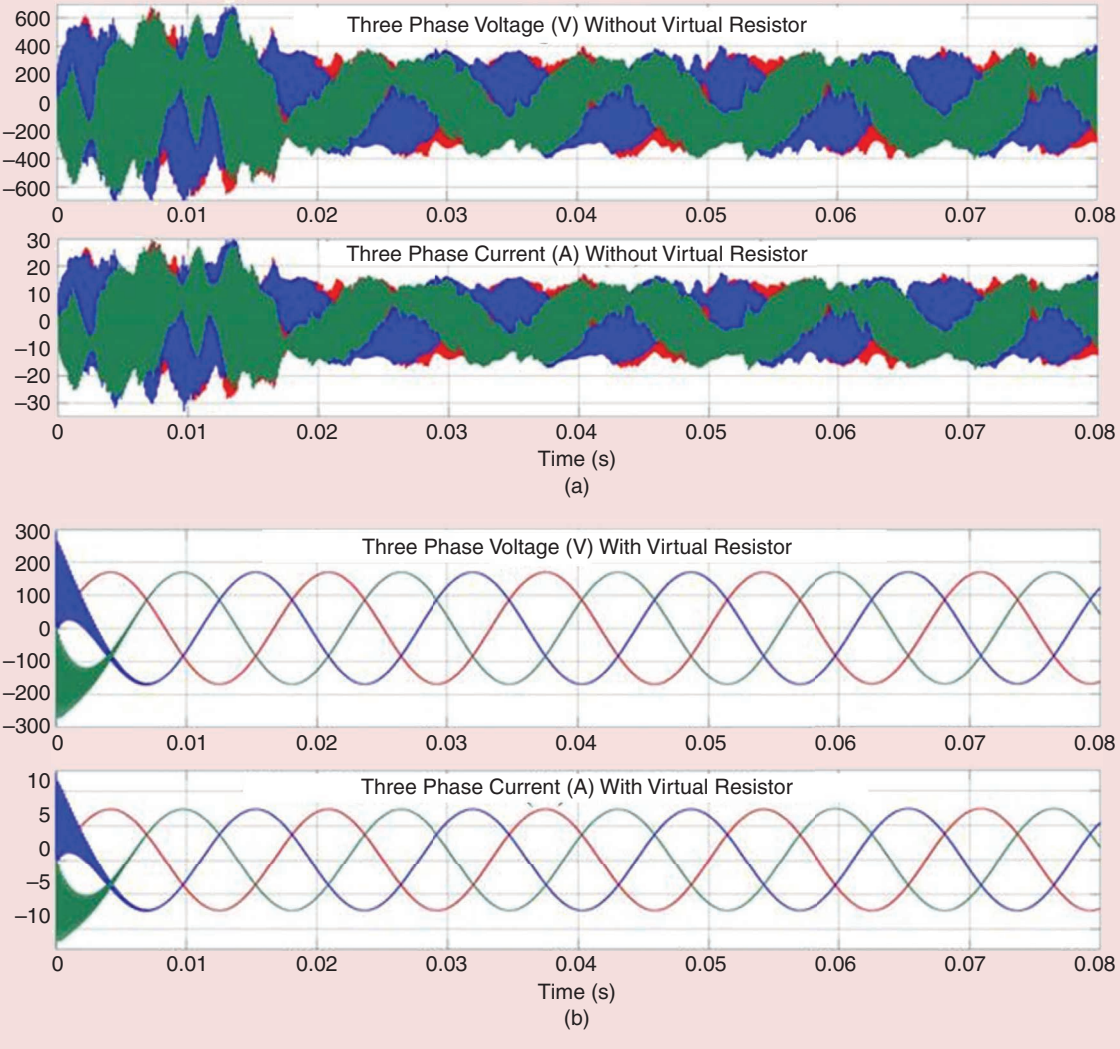

FIG 9 Simulated grid voltage for 2 kW output power. (a) without virtual resistance, (b) with virtual resistance [13].

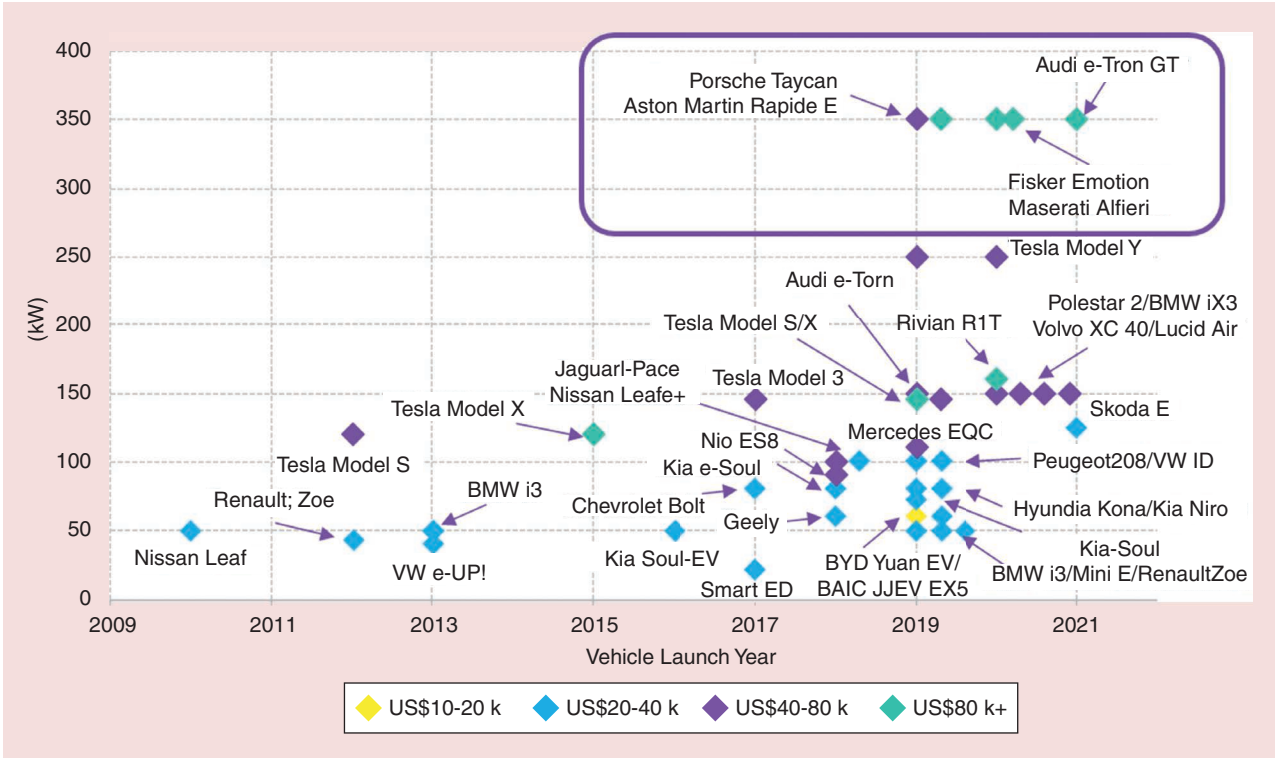

FIG 10 Comparison of EV charging capabilities [14]. Source: BloombergNEF, Company Press Releases.

to have this capability in 2020, and have delivered more than 20,000 vehicles in 2020 (Figure 10).

Because of the costs required to upgrade the utility system's infrastructure to accommodate the power levels expected with XFC, most designs require multiple XFCs to be deployed per charging site so that utility costs are spread over several charging stations. This also allows for ease in scheduling the charge demanded to avoid drawing too high peak power from the utility, creating the power cluster. On the other hand, to maximize the profitability of XFC stations, significant up-front modeling will be required to assess where to locate these within the electric system such that minimum system modifications are needed. Many have also pointed out that because of the large power required at these locations, power sources such as photovoltaics (PV) and energy storage (batteries) will need to be integrated to help reduce the demands on the grid [13], as shown in Figure 11. Some researchers have also proposed using bidirectional chargers to transfer charge among vehicles or to provide grid support when needed, but this option may face opposition from vehicle OEMs as the additional battery cycling may reduce the overall battery lifetime.

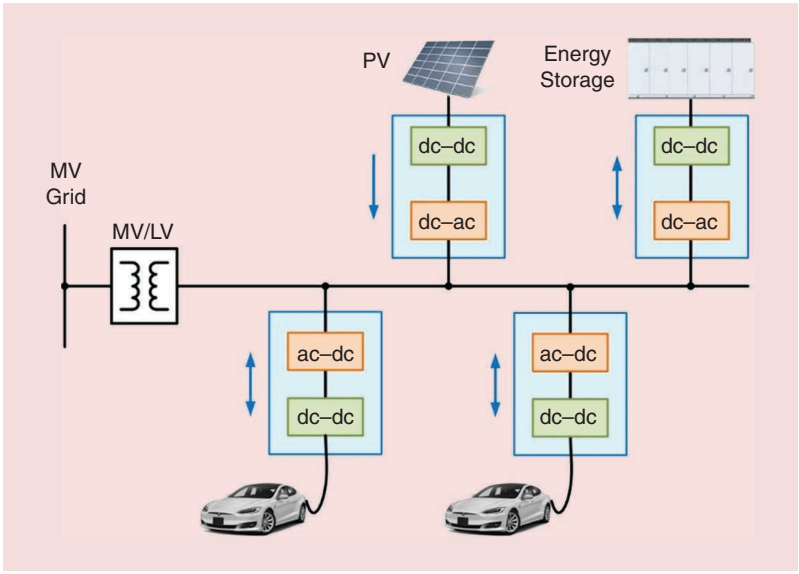

FIG 11 AC-connected XFC station [15].

One recent mission is to eliminate the MV/LV transformer (shown in Figure 11), given such high-power 50/60 Hz transformer is bulky and heavy. Thanks to the recent breakthrough with HV SiC MOSFETs (devices with voltage ratings of 10 kV), a modular design is a promising candidate such that voltage blocking can be divided among multiple devices/modules. In addition to the two-level design using >6 kV devices, [16] proposed a multilevel converter as shown in Figure 12(a). Both the PFC stage and dc-dc stage use a three-level topology as shown in the figure. 1200 V SiC MOSFETs or Si IGBTs can be used at the secondary side to save cost.

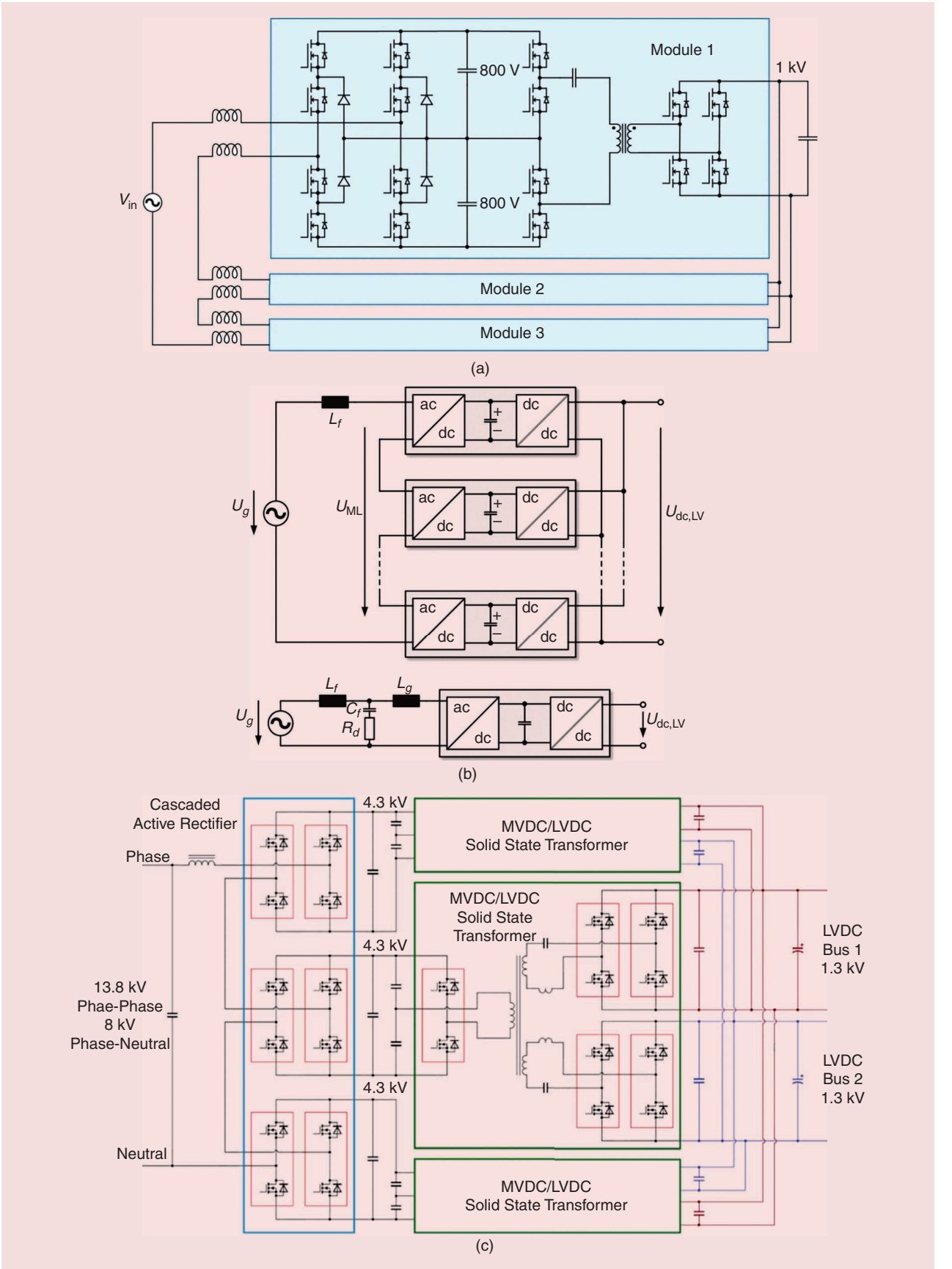

FIG 12 (a) Modular design using the multilevel (three-level) topology [16]. (b) Block diagram of an ISOP XFC [17]. (c) Exemplary design of ISOP XFC station for two vehicles [18].

Given the voltage limits of power semiconductors nowadays, input series and output parallel (ISOP) is a popular candidate as shown in Figure 12(b) [17]. Since such dc-dc stage still engages the HF transformer, here "Transformerless" actually means that no 50/60 Hz transformer is used, but instead still incorporates a high frequency [>10 kHz] transformer that is much more compact in size and weight. One exemplary ISOP XFC is presented in Figure 12(c) [18], proposed by the UTK team and Wolfspeed, under the sponsor of U.S. Department of Energy. To transfer the power, the ac voltage at the grid is first rectified and transferred to the primary side dc link, such as 4.3 kVdc which allows 6 kV SiC MOSFETs to be adopted. The number of series-connected H-bridges on the grid side is determined by the ac-grid voltage and the switch voltage rating. Then, the high-frequency inverter converts the dc voltage to high-frequency ac voltage and transfers power from the dc link to the resonant network formed by compensation components (resonant inductor and capacitors).

A MV HF transformer is needed for voltage isolation purposes. If only one car is charged from the XFC, the transformer secondary side only needs one winding. In this particular case, the XFC is designed to charge two cars simultaneously, so two secondary-side windings are used. The secondary windings then induce a stepped-down ac voltage, which will be rectified by the LV H-bridges with output voltage being paralleled forming the LVDC bus (e.g., 1.3 kVdc). To charge regular EV batteries of 200–450 Vdc, another buck converter is needed to step-down the 1.3 kVdc to the battery voltage. Note using XFC technology to charge the battery still needs to secure high quality output voltage/current at the battery side, for instance output voltage 200 – 920 V with ripple of ±5% or ±5 V, and output current up to 500 Adc with ripple <1.5 A and frequency <10 Hz, based on IEC 61851-23.

To alleviate the switching loss and transformer stress thereby avoiding the scenario in FIG 4, a typical resonant-type isolated MVDC-LVDC converter can be a good choice, e.g., an LC type also called dc transformer (DCX) converter. The resonant network only incorporates series-connected capacitors C and transformer leakage inductance L on the secondary side. The transformer mutual inductance is much larger than the leakage inductance. Therefore, it has little effect on the resonance. At the resonance frequency, this topology behaves as a constant voltage source. The transformer turns ratio can be accurately designed to transform the 4.3 kVdc bus to a 1.3 kVdc output. Essentially, such DCX topology is made to eliminate the switching losses, given the switching moments all happen around current zero crossing points, which helps in natural ZVS turn-on and zero-current switching turn-off for both primary side and secondary side switches as shown in Figure 13. In addition, the resonant topology avoids the transformer windings from having to accommodate the high dv/dt of the switches, further facilitating the transformer design.

The first major concern with this topology is its resonant capacitors. High voltages at resonant frequency are induced across the resonant capacitor. Such high voltage stress, usually multiple times of the dc-bus voltage, requires a large number of film capacitors in series and parallel, resulting in large capacitor banks. Meanwhile, such high-frequency voltage is also subject to significant EMI issues. The second major concern lies in the MV high-frequency transformer, which has issues of partial discharge. In recent years, researchers are aware of the challenge of such MV transformer design. The high dv/dt of SiC devices requires the larger distance among turns, which enlarges the size of the MV transformer.

Nevertheless, with the operating frequency of a transformer increasing, reduction of the transformer size and weight is still expected, given its core cross section is reduced inversely proportionally to the frequency. Nanocrystalline cores, for instance, can be produced with sheet thicknesses as low as 13 μm, in contrast to the 350 μm thickness of conventional grain-oriented electrical steel used at the line frequency. However, for MV insulation, the miniaturization of the transformer creates a direct challenge for the dielectric design, given increasing frequency does not reduce the clearance distance required for insulation. Meanwhile, because of the MV ratings required, the insulation material layer, which encapsulates the MV-winding and isolates it from the LV-winding and the core, has to be rather thick, which increases the transformer size again.

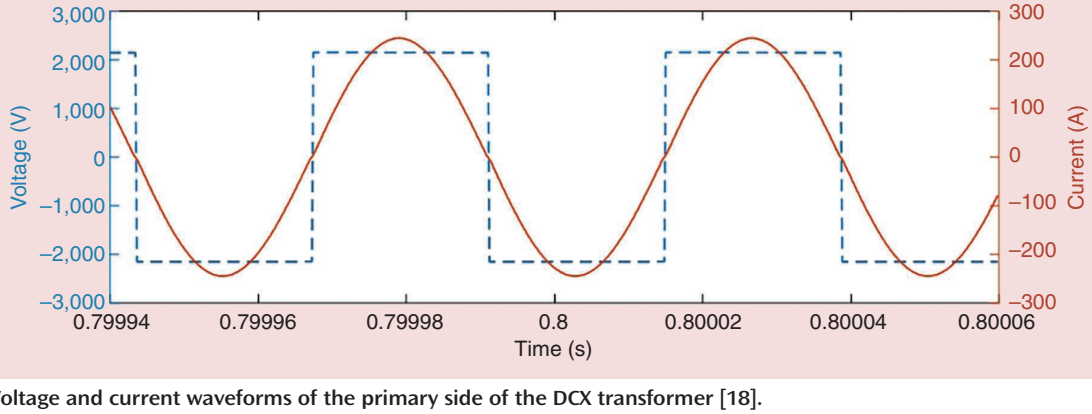

FIG 13 Voltage and current waveforms of the primary side of the DCX transformer [18].

Two main families of cores are available for MV transformer design: the powder type and the tape type. Although the powder types are generally referred to as ferrites, a variety of materials can be used in terms of loss and saturation levels. One challenge is that ferrite cores are not easily manufactured in larger sizes. Therefore, nowadays such materials are mainly applied in low-power applications. Additionally, ferrites usually have relatively low flux density saturation levels (e.g., ~0.3–0.5 T). Tape type cores, in theory, have unlimited size. Therefore, they can be produced in much larger sizes than ferrites. The main material types for these cores are amorphous, nanocrystalline, nickel iron, and cobalt iron. The main core parameters are shown in Table 1. As a summary, the XFC design challenges nowadays are more on the materials instead of power electronics control.

Wireless Charging

In 2007, a group of scientists in MIT successfully delivered 60 W at 40% efficiency over a 2 m distance between coupled coils of 30 cm radius [19]. They co-founded WiTricity later which has been working closely with major automakers like BMW and Hyundai by licensing its technology and has demonstrated a series of wireless charging prototypes for next generation vehicles. In 2018, BMW introduced the 530e iPerformance, the world's first electric sedan that is factory equipped with a wireless charger using WiTricity's techniques.

Meanwhile, Qualcomm's Halo collaborated closely with the University of Auckland and has developed a number of coil pad geometries suitable for wireless EVs, including the patent for the double D coil pad [20]. In 2019, it was acquired by WiTricity with its over 1500 patents or patent applications. Plugless Power provides wireless chargers with 3.6 – 7.2 kW power rating and allows customers to directly install the charger on their vehicles. The supported models include Telsa Model S, BMW i3, and Nissan Leaf. In 2021, HEVO licensed a series of wireless charging technologies from Oak Ridge National Laboratory (ORNL), including a unique polyphase coil structure that enables a very high coil surface power density at 1.5 MW/m^2. HEVO is working with ORNL to build a 300 kW system to meet the 15-min charging goal for EVs with 100 kWh battery packs [21].

Images of wireless chargers from different companies are given in Figure 14, with their specifications compared in Table 2. All IPT systems use inductive coupling of a magnetic field between two coils. Controlled

Table 1. Comparison of Main Core Parameters.

	Ferrite MnZn	Amorphous (iron-based)	Amorphous (cobalt-based)	Nano crystalline	Nickel iron (79%)	Cobalt iron (50%)
Core type	Powder	Tape	Tape	Tape	Powder/tape	Tape
Saturation induction at 20 °C (T)	0.43	1.56	0.57	1.23	0.88	2.1
Curie temperature (°C)	140	395	225	600	450	940
Core losses at 10 kHz (W/kg)	70.0	250.0	4.0	28.7	50.0	400.0
Saturation magnetostriction (ppm)	-0.6	27.0	1.0	0.5	12.0	70.0

(a)

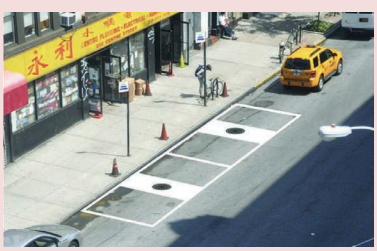

(b)

(c)

(d)

FIG 14 (a) Commercially available prototype from WiTricity. (b) Manhole-like charger from HEVO. (c) Electric bus from Momentum. (d) Customized charger from Plugless Power.

by a varying current source in the primary side coil, a predominantly magnetic time-varying field is generated between the coils. Both the coil-to-coil distance and the coil size are generally much smaller than the operating frequency's wavelength. For most of the current coil designs, Litz wire is used extensively instead of the conventional solid AWG wire for its capability of reducing high frequency eddy current loss. Usually, magnetic cores like ferrite plates or bars are applied to better channel the flux around the coil.

The typical structure of an IPT charger is shown in Figure 15. Compared to the wired charger of Figure 2, the main difference is the pair of loosely-coupled ($k \ll 1$) coils L_p and L_s that replace the transformer of the wired charger. Due to the low coupling resulting from the air gap between transmitter and receiver, impedance matching networks (IMN) are used to cancel out the large uncoupled series reactances on both coils and limit the circulating reactive power. Each IMN can be as simple as a single capacitor designed to resonate with the coil inductance, either in series or in parallel. In either event, the IMN gives the system a bandpass characteristic and results in a dominantly single-frequency magnetic field between the two coils. Differences in series or parallel compensation, resonating with coil self-inductance or uncoupled inductance, or the use of more complex IMNs such as LCC of LCL networks will influence the charger's dynamics, harmonic attenuation, and loading of the inverter and rectifier over varying output power levels and misalignment conditions [23], [24].

Different coil pad structures have been explored in the literature, mainly including circular, rectangular, DD, and DDQ pads. To have a fair and comprehensive comparison on the system performance using different coil pad structures, a multi-objective optimization is developed in [22] considering the tradeoffs between conflicting design parameters to evaluate and compare the performance of different coil pad structures. The main conclusions are:

a) Circular pads have the highest coupling coefficient and efficiencies for the same gravimetric power density under the perfectly aligned condition.
b) Circular pads use the most ferrite and the least copper for the same system performance.
c) Polarized pads including DD and DDQ give better misalignment performance in the longitudinal direction.
d) Both circular and rectangular pads have lower stray field densities compared to polarized pads.

In CPT, energy is delivered through coupled metal plates instead of coupled inductors. Compared with IPT, CPT features favorable characteristics including lightweight and cost-effective design. It does not require expensive high-frequency Litz wires or heavy magnetic cores, which aids the high frequency design to reduce the weight of passive components. However, CPT suffers from two major issues: low coupling capacitance and high fringing field. Capacitive coupling requires a relatively large coupling area to achieve large coupling capacitance, imposing a design challenge on high power density. For high power EV applications with a large air gap, the transmission efficiency is low due to the low coupling capacitance between the paralleled plates. To compensate, MHz operating frequencies are required to reduce the impedance, which directly imposes a design challenge for the high power, high frequency converters. In addition, relatively large-valued microhenry-range inductances are required for resonant matching networks in the MHz frequency range, leaving a design challenge for high value, high quality factor inductors at high frequency. The high fringing field at the edge of coupled metal plate pairs is another concern for CPT because of electric field exposure limits on the human body.

Whether using CPT or IPT, maximum power and coupler design are constrained by electromagnetic compliance and human exposure. EMC requirements, both regulatory and system-level, are similar in WPT systems to traditional wired chargers. The near-field electric and/or magnetic fields used to transfer power are minimally radiative, though the long coils and large conductors used may make radiated compliance difficult when higher harmonics are

Table 2. Industrial Wireless EV Charger Specifications.

Company	Frequency [kHz]	Airgap [mm]	Power rating [kW]	Efficiency
WiTricity	145	180	3.3–11	90–93%
Momentum	NA	610	50–200	NA
HEVO	85	305	1–10	>85%
Plugless Power	20	152	3.3–7.2	89%
WiPowerOne	85	200	27	80%

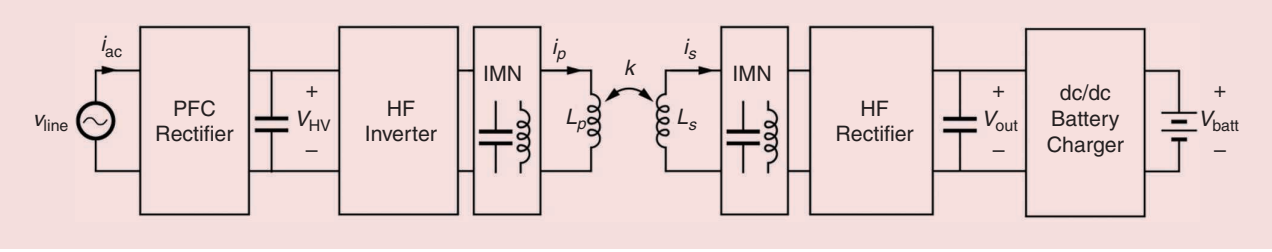

FIG 15 Typical structure of an IPT charger for EVs.

present. The risk of human exposure, however, is unique to WPT. Incidental exposure can occur near the sides or bumper of the vehicle during charging. Guidelines set forth by the International Commission on Non-Ionizing Radiation Protection (ICNIRP) give reference levels for general public exposure to time-varying fields, including a limit of 27 μT rms magnetic field exposure in the frequency range from 3 kHz to 10 MHz [25], with additional considerations required for frequencies above 100 kHz [26]. The geometric design of the coil, ferrites, and conductive shielding elements (including the vehicle underbody) are required to ensure any possible human exposure remains below safe reference levels, even under misalignment.

Particularly for IPT, foreign metallic objects present an additional concern. Eddy currents induced in metallic objects due to the magnetic fields can cause dangerous heating and ignition risk, e.g., gum wrappers, cans, or staples. If the system cannot be designed with sufficiently small magnetic fields to prevent ignition, foreign object detection (FOD) sensing and control schemes are required [27].

The SAE J2954 specifies a multitude of design, communication, and testing procedures for light-duty wirelessly-charged EVs. Standardization facilitates interoperability of dissimilar coil geometries and designs, and provides a common reference assessment for safety, EMC, and performance under misalignment. These benefits come at the cost of a limited design space, in particular due to the 85 kHz frequency used for powers below 11 kW. Compliance with SAE J2954 is not required, however, proliferation of wireless charging in EVs will benefit from the interoperability afforded by standardization.

Figure 16 summarizes the state-of-the-art WPT systems for EV charger applications from both the industry and academia. The color of dot represents the WPT technique applied. Critical performance specifications are also labeled, including system dc-dc efficiency, coil power density and power transfer distance. Compared to CPT, IPT is a relatively mature technology for WPT systems for EV chargers with air gap up to dozens of centimeters with power rating up to tens of kilowatts. Most use frequencies below 100 kHz, many of which use 85 kHz following SAE J2954. The highest coil surface power density of the reviewed works is 250 kW/m^2 achieved by the 88.5 kHz, 50 kW three-phase series-compensated coil in [28].

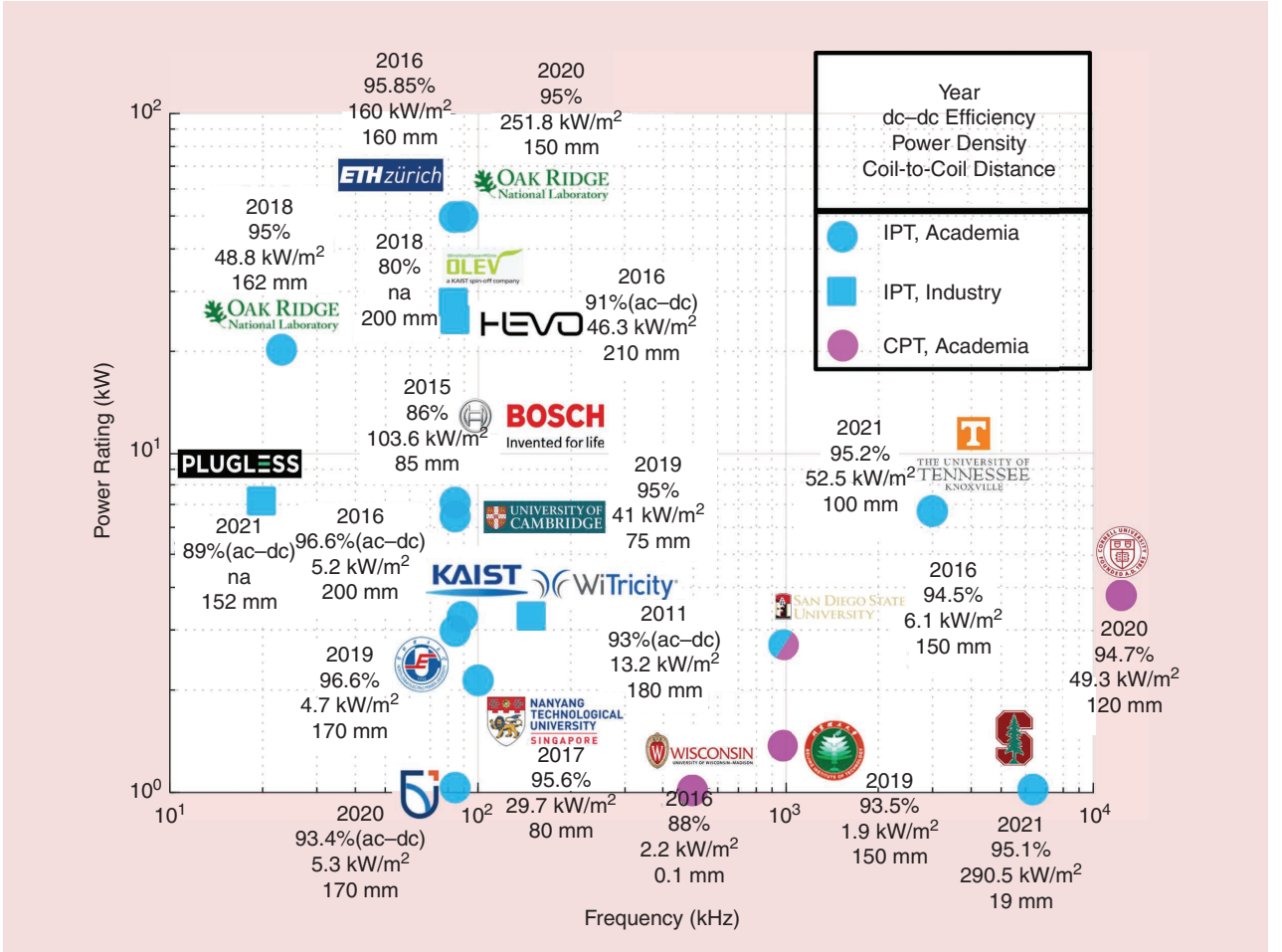

FIG 16 State-of-the-art WPT systems for EV charging.

High frequency WPT system designs at frequencies above 1 MHz have also been explored, enabled by wide bandgap devices. High frequency operation does not inherently benefit the system, but enables the use of new self-resonant (SR) passive component designs, which have the potential to reduce weight and volume of the system. Compared to coils made of Litz wires, the SR coil has many advantages including its compact structure without need for lumped compensation capacitors [29], [30]

For the further adoption of WPT for EVs in the industry, there are still economics challenges brought by the infrastructure costs including the magnetic couplers, power electronics, and energy consumption [23]. The unique requirement of high power delivery over 100 – 250 mm airgap makes WPT system efficiency relatively low compared to the wired EV chargers with similar power ratings. The state-of-the-art EV WPT charger products exhibit only 90 – 93% efficiency, which brings challenge in both energy costs and thermal management design of the system. For a better power transfer with higher efficiency, the couplers' size is often larger than 50 cm in diameter, inevitably increasing the material cost and total weight. Considering all the factors above, more innovative coil structures and more advanced WPT system design methods are still needed. High efficiency, high power density, lightweight WPT systems with low cost are imperative for increased adoption of wireless EV charging in the future.

Conclusions

Authors have been engaged in EV charging techniques for more than a decade. While witnessing the low-power charger development is approaching the design plateau, power electronics engineers now must examine other parts of the EV for further optimization, such as integrating charger with other on-board systems to save the cost and size, to engage the charger more with the power grid, and to further increase the charging power or efficiency of WPT systems.

In addition to what has been discussed in this paper, there are many other aspects of EV charging technologies to explore; for instance, the impact of various charging algorithms on the battery lifespan, and selection of the cables and associated cooling techniques for the XFC.

While this article is focused on 400 V battery charging, in reality charging a 48 V battery in electric shuttles or >800 V battery for heavy duty vehicles are not rare cases. In fact, with power demand increasing for EVs, it is projected 800 V battery will become the mainstream in the near future. Even for a conductive XFC station, during non-charging period the PFC converter can provide grid services such as reactive power generation for voltage regulation. The charger development then becomes more interdisciplinary, diverging from conventional power electronics design to interacting with power system and material science.

About the Authors

Hua (Kevin) Bai received the B.S. and Ph.D. degrees in electrical engineering from Tsinghua University, Beijing, China in 2002 and 2007, respectively. He was an assistant professor in Department of Electrical and Computer Engineering, Kettering University, MI, USA from 2010~2016. In 2017~2018, he joined University of Michigan-Dearborn as an associate professor. He is currently an associate professor in the Department of Electrical Engineering and Computer Science at The University of Tennessee, Knoxville, USA. His research interests include power electronics modeling, control, and integration including variable frequency motor drive systems, high-voltage and high-power dc/dc converter, electric vehicle battery chargers and various wide-bandgap device applications.

Daniel Costinett received the Ph.D. degree in electrical engineering from the University of Colorado Boulder in 2013. He is currently an associate professor in the Department of Electrical Engineering and Computer Science at the University of Tennessee, Knoxville, USA. His research interests include resonant and soft switching power converter design, high efficiency wired and wireless power supplies, on-chip power conversion, medical devices, and electric vehicles.

Leon M. Tolbert received the Bachelor's, M.S., and Ph.D. degrees in electrical engineering from the Georgia Institute of Technology, Atlanta, in 1989, 1991, and 1999, respectively. He is currently a Chancellor's Professor and the Min H. Kao Professor in the Department of Electrical Engineering and Computer Science, The University of Tennessee, Knoxville, USA. He is also an adjunct participant with Oak Ridge National Laboratory, where he previously worked from 1991 to 2020. His research interests include the utility applications of power electronics, microgrids, electric vehicles, and wide bandgap semiconductors.

Ruiyang Qin received his B.S. degree in Automation with joint program from Shanghai Jiao Tong University and University of Pennsylvania in 2013, M.S. degree from Virginia Tech in 2016, and PhD degree from the University of Tennessee, Knoxville, USA, in 2022. His research interests include high quality factor self-resonant coil design for wireless power transfer, and high-frequency WBG-based wireless power transfer system for EV applications.

Liyan Zhu received his BS degree in Department of Electrical Engineering of Kunming University of Science and Technology, Kunming, China in 2017. He is currently working toward the Ph.D. degree with the Center for Ultra-wide-Area Resilient Electric Energy Transmission Networks (CURENT), The University of Tennessee, Knoxville, TN, USA. His research interests include WBG device-based dc/dc converters, magnetic components, fast chargers, auxiliary power modules and integrated chargers in EV.

Ziwei Liang received the B.S. and M.S. degrees in electrical engineering from the China University of Mining and Technology, Xuzhou, China, and the Beijing Institute of Technology, Beijing, China, in 2016 and 2018, respectively. He is currently working towards the Ph.D. degree with the

Department of Electrical and Computer Engineering, The University of Tennessee, Knoxville, TN, USA. His research interests include EV chargers and wireless power transfer.

Yang Huang received the B.S. degree from Southeast University, Nanjing, China in 2016, and the M.S. degree from the University of Michigan-Dearborn, MI, USA in 2018. He is currently pursuing a Ph.D degree in the Department of Electrical Engineering & Computer Science, The University of Tennessee-Knoxville, TN, USA. His research interests include on-board EV charger and fast charger design, FPGA based controller design, motor drive techniques and common-mode noise reduction.

References

[1] A. Emadi, S. S. Williamson, and A. Khaligh, "Power electronics intensive solutions for advanced electric, hybrid electric, and fuel cell vehicular power systems," *IEEE Trans. Power Electron.*, vol. 21, no. 3, pp. 567–577, May 2006, doi: 10.1109/TPEL.2006.872378.

[2] L. Kostal, L. Schmidhauser, L. Kabel, and R. Bosch, "Voltage casses for electric mobility," German Electrical and Electronic Manufacturer's Association, 2013.

[3] C. Jung, "Power up with 800-V systems: The benefits of upgrading voltage power for battery-electric passenger vehicles," *IEEE Electrif. Mag.*, vol. 5, no. 1, pp. 53–58, Mar. 2017, doi: 10.1109/MELE.2016.2644560.

[4] International standard IEC 61215-1:2016, IEC/TC82, 2016.

[5] "SAE electric vehicle and plug in hybrid electric vehicle conductive charge coupler," SAE International, J1772, 2010.

[6] R. Hou, "Evaluation of integrated active filter auxiliary power modules in electrified vehicle applications," McMaster Univ., Hamilton, Canada, 2015.

[7] C. L. Zhu, M. Shen, and M. Obrigkeit, "A high power DC/DC converter designed for single coolant loop hybrid electric vehicle application," SAE Technical Papers, 2010-01-1254, 2010.

[8] O. García, L. A. Flores, J. A. Oliver, J. A. Cobos, and J. De La Peña, "Bidirectional dc-dc converter for hybrid vehicles," in *Proc. PESC Rec. – IEEE Annu. Power Electron. Specialists Conf.*, 2005, pp. 1881–1886.

[9] A. Emadi, *Advanced Electric Drive Vehicles*. Boca Raton, FL, USA: CRC Press, 2014.

[10] S. Y. Kim, I. Jeong, K. Nam, and H. S. Song, "Three-port full bridge converter application as a combined charger for PHEVs," in *Proc. 5th IEEE Veh. Power Propulsion Conf. (VPPC '09)*, 2009, pp. 461–465.

[11] H. Tao, A. Kotsopoulos, J. L. Duarte, and M. A. M. Hendrix, "Triple-half-bridge bidirectional converter controlled by phase shift and PWM," in *Proc. IEEE Appl. Power Electron. Conf. Expo. (APEC)*, 2006, vol. 2006, pp. 1256–1262, doi: 10.1109/APEC.2006.1620700.

[12] L. Zhu, H. Bai, A. Brown, and L. Keuck, "A current-fed three-port DC/DC converter for integration of on-board charger and auxiliary power module in electric vehicles," in *Proc. Appl. Power Electron. Conf. Expo. (APEC)*, 2021, pp. 577–582, doi: 10.1109/APEC42165.2021.9487263.

[13] Y. Fu *et al.*, "Design methodology of a three-phase four-wire EV charger operated at the autonomous mode," *IEEE Trans. Transp. Electrific.*, vol. 5, no. 4, pp. 1169–1181, 2019, doi: 10.1109/TTE.2019.2957635.

[14] "Will ultra-fast charging take-off? (Part one)," BNEF, 2019.

[15] H. Tu, H. Feng, S. Srdic, and S. Lukic, "Extreme fast charging of electric vehicles: A technology overview," *IEEE Trans. Transp. Electrific.*, vol. 5, no. 4, pp. 861–878, 2019, doi: 10.1109/TTE.2019.2958709.

[16] C. Zhu, "High-efficiency medium-voltage-input, solid-state-transformer -based 400-kW/1000-V/400 – A extreme fast charger for electric vehicles [Web page PowerPoint]," Delta Electronics (Americas) Ltd., Jun. 13, 2019. [Online]. Available: www.energy.gov/sites/prod/files/2019/06/f64/elt241_zhu_2019_o_4.24_9.31pm_jl.pdf

[17] D. Rothmund, T. Guillod, D. Bortis, and J. W. Kolar, "99.1% efficient 10 kV SiC-based medium-voltage ZVS bidirectional single-phase PFC AC/DC stage," *IEEE J. Emerg. Sel. Topics Power Electron.*, vol. 7, no. 2, pp. 779–797, 2019, doi: 10.1109/JESTPE.2018.2886140.

[18] Z. Liang, D. Merced, M. Jalalpour, and H. Bai, "Deployment of a bidirectional MW level electric-vehicle extreme fast charging station enabled by high-voltage SiC and intelligent control," *Energies*, vol. 13, no. 7, p. 13, 2020, doi: 10.3390/en13071840.

[19] A. Kurs, A. Karalis, R. Moffatt, J. D. Joannopoulos, P. Fisher, and M. Soljacic, "Wireless power transfer via strongly coupled magnetic resonances," *Science*, vol. 317, no. 5834, pp. 83–86, Jul. 6, 2007, doi: 10.1126/science.1143254.

[20] G. Covic and M. Budhia, "Flux coupling device and magnetic structures therefor," U.S. Patent 10 878 995 B2, Dec. 29, 2020.

[21] "High-power wireless vehicle charging technology licensed by HEVO," Oak Ridge National Lab., Aug. 2021. [Online]. Available: https://www.ornl.gov/news/high-power-wireless-vehicle-charging-technology-licensed-hevo

[22] S. Bandyopadhyay, P. Venugopal, J. Dong, and P. Bauer, "Comparison of magnetic couplers for IPT-based EV charging using multi-objective optimization," *IEEE Trans. Veh. Technol.*, vol. 68, no. 6, pp. 5416–5429, 2019, doi: 10.1109/TVT.2019.2909566.

[23] D. Patil, M. K. McDonough, J. M. Miller, B. Fahimi, and P. T. Balsara, "Wireless power transfer for vehicular applications: Overview and challenges," *IEEE Trans. Transp. Electrific.*, vol. 4, no. 1, pp. 3–37, Mar. 2018, doi: 10.1109/TTE.2017.2780627.

[24] H. Feng, R. Tavakoli, O. C. Onar, and Z. Pantic, "Advances in high-power wireless charging systems: Overview and design considerations," *IEEE Trans. Transp. Electrific.*, vol. 6, no. 3, pp. 886–919, Sep. 2020, doi: 10.1109/TTE.2020.3012543.

[25] International Commission on Non-Ionizing Radiation Protection, "Guidelines for limiting exposure to time-varying electric and magnetic fields (1 Hz to 100 kHz)," *Health Phys.*, vol. 99, no. 6, pp. 818–836, 2010.

[26] International Commission on Non-Ionizing Radiation Protection, "Guidelines for limiting exposure to electromagnetic fields (100 kHz to 300 GHz)," *Health Phys.*, vol. 118, no. 5, pp. 483–524, 2020.

[27] Y. Zhang, Z. Yan, J. Zhu, S. Li, and C. Mi, "A review of foreign object detection (FOD) for inductive power transfer systems," *eTransportation*, vol. 1, Aug. 2019, Art. no. 100002, doi: 10.1016/j.etran.2019.04.002.

[28] J. Pries, V. P. N. Galigekere, O. C. Onar, and G. Su, "A 50-kW three-phase wireless power transfer system using bipolar windings and series resonant networks for rotating magnetic fields," *IEEE Trans. Power Electron.*, vol. 35, no. 5, pp. 4500–4517, May 2020, doi: 10.1109/TPEL.2019.2942065.

[29] L. Gu, G. Zulauf, A. Stein, P. A. Kyaw, T. Chen, and J. M. R. Davila, "6.78-MHz wireless power transfer with self-resonant coils at 95% DC–DC efficiency," *IEEE Trans. Power Electron.*, vol. 36, no. 3, pp. 2456–2460, Mar. 2021, doi: 10.1109/TPEL.2020.3014042.

[30] R. Qin, J. Li, and D. Costinett, "A 6.6-kW high-frequency wireless power transfer system for electric vehicle charging using multilayer nonuniform self-resonant coil at MHz," *IEEE Trans. Power Electron.*, vol. 37, no. 4, pp. 4842–4856, Apr. 2022, doi: 10.1109/TPEL.2021.3120734.

PEM